A high performance graphene/few-layer InSe photo-detector

Zhesheng Chen, Johan Biscaras, Abhay Shukla

High performance graphene/few-layer InSe photo-detector

Zhesheng Chen, [a,b] *Johan Biscaras,*[a] *and Abhay Shukla* *[a]

[a]Institut de Minéralogie, de Physique des Matériaux, et de Cosmochimie (IMPMC), Sorbonne Universités - UPMC Univ Paris 06, UMR CNRS 7590, MNHN, IRD UMR 206, 4 Place Jussieu, F-75005 Paris, France.

[b]School of Nuclear Science and Technology, Lanzhou University, Lanzhou 730000, PR China.

ABSTRACT: We fabricate a graphene/few-layer InSe heterostructure photo-detector and solve a recurrent materials problem concerning degradation of ultra-thin atomic layers in air. This heterostructure has a largely enhanced performance explained by its fundamentally different mode of functioning with respect to the corresponding device without graphene.

Photo-detectors are expected to be one of the first applications of two dimensional (2D) materials because of the extraordinary electric and optical properties obtained in one or few atomic layers of such materials.[1-4] As the prototype 2D material, graphene has high carrier mobility, a broad absorption spectrum and fast response time which are vital ingredients for high performance photo-detectors.[5] However, the weak absorbance of graphene is a strong limitation and the highest photoresponsivity based on an exfoliated graphene photo-detector is 6.1 mA/W to date.[6]

Recently, the successful fabrication of few-layer 2D transition metal dichalcogenide semiconductors (TMDCs) with much larger optical absorption has raised this limit by several orders of magnitude and thus largely improved photo-detector performance.[7,8] For example, the photoresponsivity of a photo-detector based on exfoliated monolayer MoS_2 is found to be 880 A/W at 561 nm.[9] The electronic band gap of TMDCs can also be tuned in some cases between indirect and direct as a function of the number of layers, a fact that could be crucial for designing efficient photo-detectors.[10] Carrier mobility in these semiconductors being relatively low compared with graphene, efficiency can suffer due to fast recombination of photo-excited electron-hole pairs, leaving room for further improvement. With this in mind, devices were fabricated with graphene decorated with PbS quantum dots to combine the conversion efficiency of the semiconductor with the charge transport characteristics of graphene.[11] Atomically thin graphene/MoS_2 heterostructures motivated by similar considerations also showed a photoresponsivity improvement of several orders of magnitude.[12,13]

More recently, photo-detectors based on few-layer InSe (III-VI compound) have been reported,[14,15] the material being considerably different from TMDCs such as MoS_2 and WS_2. The band gap of monolayer InSe is indirect but evolves into a direct gap in roughly seven layers and above and varies from 1.26 eV to 1.45 eV according to the number of layers.[16] In MoS_2 on the contrary the monolayer has a direct band gap which transforms to an indirect band gap in bilayers and above.[10] However ultra-thin InSe has a strong limitation in that it is unstable to exposure to air or liquids unlike MoS_2.[17] This is a constraint on studying the properties or possible applications of ultra-thin InSe, but could be solved by graphene encapsulation.[18,19] In this work we transfer graphene on top of mechanically exfoliated ultra-thin InSe and study stability in ambient conditions. In addition, we fabricate graphene/few-layer InSe heterostructure and analyze the performance of a photo-detector based on this structure. There are two advantages of this heterostructure: First, ultra-thin InSe is protected by the hermetic, covering graphene which makes the device stable in air. Second, the performance of the graphene/few-layer InSe photo-detector is greatly enhanced compared with a few-layer InSe photo-detector.

We used high quality graphite and a synthetic InSe single crystal for preparation of samples and fabrication of photo-detector devices. Ultra-thin (4~5 layers) and few-layer (~20 layers) InSe were prepared onto SiO_2 (300 nm)/Si substrate by classical mechanical exfoliation. Monolayer graphene was prepared on soda-lime glass by the anodic bonding method.[20-22] After preparation, the monolayer graphene was transferred to the substrate already carrying the InSe sample as described below using the wedging transfer process.[23] During the transfer process, cellulose

acetate butyrate (CAB) solution (35 mg/mL in ethyl acetate) was spin coated on graphene on glass at 1000 rpm for 10 seconds and then 3000 rpm for 60 seconds. The solution coated glass substrate was then baked on a hot plate at 100°C for 2 minutes to dry CAB quickly. The CAB supported graphene was then transferred onto InSe on the SiO_2/Si substrate by precise alignment using micro-manipulators after dipping into de-ionized water. The same baking step was again applied to remove the residual water between the polymer and the substrate. The CAB polymer was dissolved in ethyl acetate and the heterostructure was annealed in vacuum at 250°C for 6 hours. Electrical contacts for the graphene/few-layer InSe photo-detector, were fabricated by electron beam lithography followed by evaporation of Cr (5 nm) and Au (80 nm) on top of graphene. The fabrication process of the photo-detector based on graphene/20-layer InSe heterostructure is shown in ESI (Fig. S1†) along with additional details about characterization and measurement.

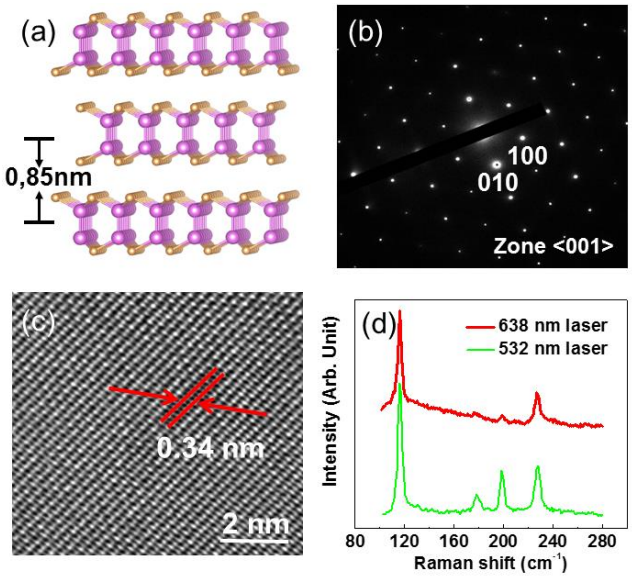

Figure 1. (a) ε polytype crystal structure of InSe with the c-axis vertical. Orange and purple spheres represent Se and In atoms respectively. (b) TEM SAED pattern of 10-layer InSe with the beam parallel to the *c* axis (c) The corresponding HR-TEM of InSe on a holey carbon grid with the lattice spacing of 0.34 nm. (d) Raman spectra of 12-layer InSe on SiO_2/Si substrate.

There are three polytypes (β, γ and ε) of layered InSe, which result from the particular stacking sequence of primitive layers.[24,25] The β and ε polytypes have the same lattice parameters (*a*=*b*=4.05Å, *c*=16.93Å) with a hexagonal unit cell comprising eight atoms extended over two layers. However, the space groups are different, non-symmorphic D_{6h}^4 group for the β polytype and symmorphic D_{3h}^1 group for the ε polytype respectively. The γ polytype, with the lattice parameters *a*=*b*=4.05Å, *c*=25.32Å, has a rhombohedric unit cell and contains four atoms distributed on four adjacent layers which belongs to the symmorphic C_{3v}^5 group. To distinguish between ε and γ polytypes we use transmission electron microscopy (TEM). Figure 1(a) shows the structure of the ε polytype in few-layer InSe, in which the thickness of the monolayer is 0.85 nm. Figure 1(b) and (c) show the selected area electron diffraction (SAED) pattern and the corresponding high resolution (HR) TEM of 10-layer InSe, prepared by mechanical exfoliation and transferred to a TEM grid. The sample is oriented with the <001> zone axis parallel to the electron beam. The spatial frequency measured for the first reflections is 0.294 $Å^{-1}$, and is therefore compatible with the position of the 100 diffraction spot of both β and ε polytypes. HR-TEM also allows a direct measurement of the d-spacing of 0.34 nm which is coherent with the {100} plane family of β and ε InSe. In the γ polytype, the extinction of *hkl* reflections with -*h*+*k*+*l*≠3n implies that the first observable reflection for this zone axis should be (110), corresponding to a spatial frequency of 0.5 $Å^{-1}$, which is not compatible with the experimental diffraction pattern. In conclusion, we can exclude the γ polytype, but SAED cannot distinguish

between β and ε polytypes. Raman spectroscopy can discriminate between these through a mode around 200 cm^{-1} which is present in the ε polytype but absent in the β polytype.[26] To exclude the possibility of mode activation by on or off-resonance conditions[27] both 532 nm and 638 nm wavelength excitation were used on exfoliated twelve-layer samples as shown in figure 1(d). We observe the 202 cm^{-1} mode in each case with intensity stronger than the E^1_{2g} mode at 178 cm^{-1}. This conclusively indicates that our few-layer samples are of the ε polytype.

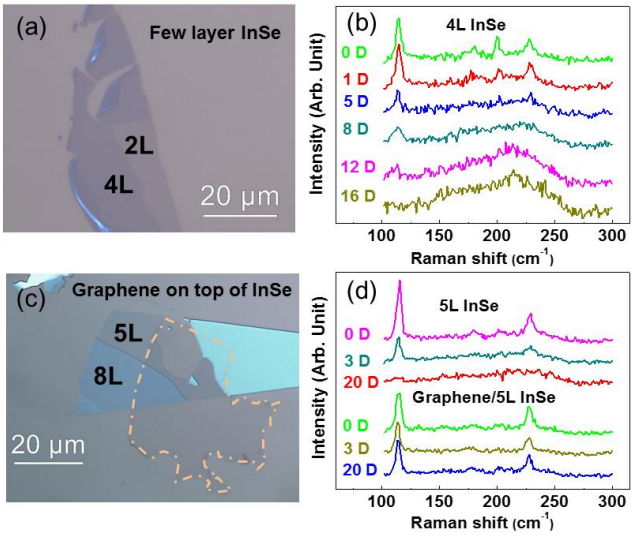

Figure 2. (a) Optical image of few-layer InSe prepared on SiO_2/Si using mechanical exfoliation. (b) The corresponding instability of 4-layer InSe in ambient conditions characterized by Raman spectroscopy. (n D: after n days) (c) Optical image of few-layer InSe partly encapsulated by the top monolayer graphene, the graphene is demarcated by an orange dashed line. (d) Raman spectroscopy comparison of stability of 5-layer InSe in ambient conditions with and without graphene protection. (n D: after n days)

Monolayer or ultra-thin 2D materials can be unstable to exposure to air or liquids.[18] Monolayer graphene and TMDCs such as MoS_2 are stable under ambient conditions, as opposed to few-

layer GaSe (III-VI layered semiconductor) which can be rapidly degraded in air.[28] We analyzed the stability of a 4-layer InSe sample as a function of exposure time in air as shown in figure 2(a-b). After sample preparation by mechanical exfoliation, the Raman modes at 114.8 cm^{-1}, 178.1 cm^{-1}, 202.1 cm^{-1} and 227.3 cm^{-1} are clearly seen. However, the intensity of these modes decreases and the modes merge fast into a rising background ranging from 150 cm^{-1} to 250 cm^{-1} when the sample is left in air over twelve days. All the Raman modes disappear after sixteen days which indicates that 4-layer InSe is degraded completely in ambient conditions. This practical problem of degradation can restrict the application of ultra-thin InSe. Following earlier work of graphene use for countering corrosion, [18,19] we transfer graphene on top of 5-layer InSe as shown in figure 2(c). In figure 2(d) Raman spectra are shown simultaneously for bare 5-layer InSe and graphene covered 5-layer InSe. The bare 5-layer InSe is degraded completely within twenty days. However, for the 5-layer InSe covered by graphene, the Raman signal remains unchanged. We conclude that a graphene covering layer is also an effective packaging material to protect ultra-thin InSe from degradation in ambient conditions.

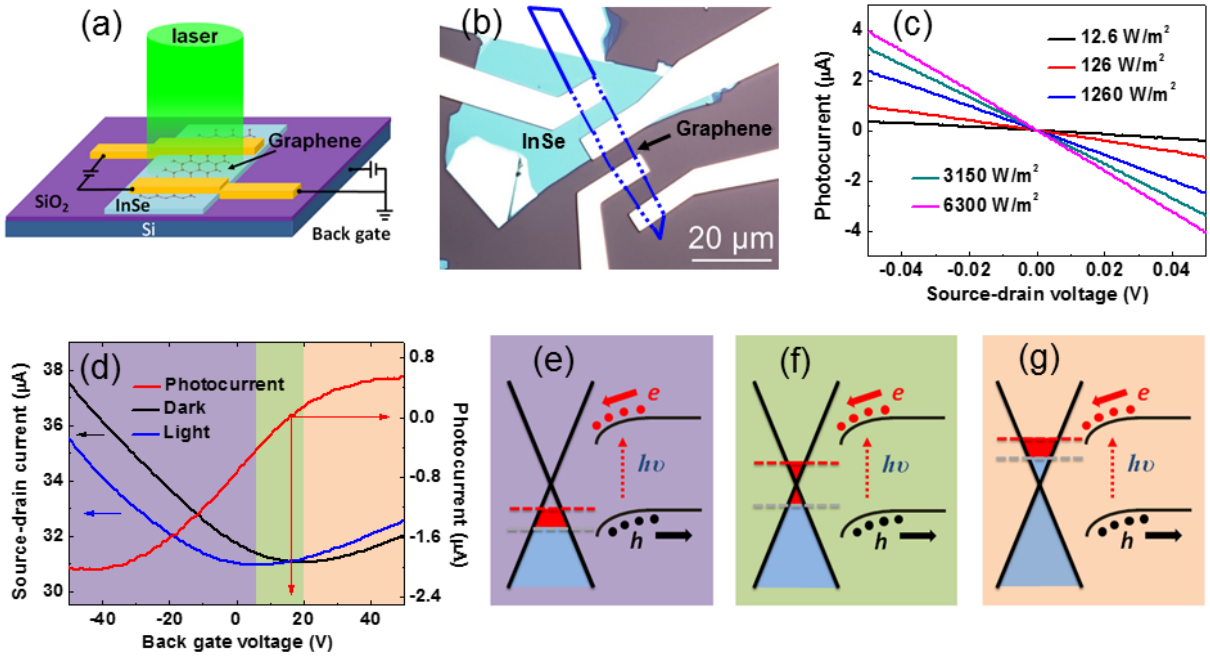

Figure 3. (a) Schematic diagram of our photo-detector based on graphene/InSe heterostructure. (b) Optical image of the device. Graphene is demarcated by the blue line. (c) Photocurrent characterization as a function of source-drain voltage for different illumination intensities and without gate voltage. (d) Source-drain current of the device in dark and illuminated conditions as a function of gate voltage. The source-drain voltage is 100 mV and the illumination power is 12.6 W/m^2. (e-g) Schematic band structure diagram of graphene/InSe heterostructure in different gate voltage regions.

We now fabricate a graphene/few-layer InSe heterostructure photo-detector and characterize it with 532 nm light illumination as schematized in figure 3(a). The optical image of the device based on a graphene/20-layer InSe heterostructure on a SiO2/Si substrate is shown in figure 3(b). We use 20 layers as a compromise between the need to use ultra-thin material for the vertical

geometry and the need to increase absorption. In figure 3(c) we show the photocurrent as a function of source-drain voltage (Vds) by varying the illumination power and with gate voltage Vg=0 V. As explained below, we are thus in the regime of negative photocurrent (purple region of figure 3(d)). Figure 3(d) shows the source-drain current through the top graphene layer as a function of the gate voltage for the dark device (black line) and the illuminated device (blue line). The photocurrent, which is the difference between these two, is shown by the red line. It can be immediately seen that this photo-detector works in a differential mode by shifting the transfer curve due to charge generated in the InSe layer. Photocarrier generation in graphene is inefficient and the current in an isolated graphene layer changes little between the dark and illuminated conditions, contrary to classical semiconductor based photo-detectors. However for the graphene layer placed on top of InSe, the charge neutral point (CNP) undergoes considerable shift with photogeneration of electron-hole pairs in InSe. The vertical geometry and the interface electronic structure make for efficient transfer of electrons to the graphene layer while holes remain trapped in the InSe layer.

A rough estimation of this increase in efficiency can be made by comparing active volumes between the heterostructure and the few-layer InSe device. In the former, the whole graphene/few-layer InSe interface is active for vertical charge extraction, whereas in the latter only the regions within a mean free path of source or drain contacts permit lateral charge extraction (schematics in ESI, Fig. S5†). Using the devices measured in this work and mean free paths of ~5 nm in the lateral direction and ~2 nm in the vertical direction in InSe,[29] we find an

active volume 10^3 times higher in the heterostructure which gives an estimation of the increase in efficiency expected in this device.

In figure 3(e-g) we show schematic band diagrams of the graphene/few-layer InSe interface for various regimes of the device as defined by the gate voltage. The work functions of graphene and InSe are different (4.56 eV and 5.2 eV respectively)[30,31] and when the two materials are in contact the Fermi levels must coincide at the interface. The electronic bands of InSe bend as a consequence. Considering figure 3(d) again, we notice firstly that the CNP for the graphene layer in the dark device is at 20 V which indicates hole doping, probably introduced by the transfer process and confirmed through the measurements of Raman shifts (ESI, Fig. S3†). As noted above, the CNP shifts under illumination to 6 V which means that graphene is now less hole doped. Electrons generated by illumination in InSe flow into graphene, nearly compensating the initial hole doping.

Therein lies the mechanism for generating ample photocurrent as the difference between these two shifted transfer curves for the top graphene layer. This is also the reason why the photocurrent changes sign,[12] a phenomenon not observed in InSe or other homostructural photo-detectors.[14,15,32] The Fermi levels in graphene are shown in figures 3(e-g) by a grey line (dark device) and a red line (illuminated device), the illuminated Fermi level always being at higher energy as a result of the electrons flowing in from the InSe. In the central green shaded region of figure 3(d) the Fermi level of graphene for the dark device varies between the neutral point and slight hole doping while the Fermi level of graphene for the illuminated device varies between

neutrality and slight electron doping. The particular case of zero photocurrent is illustrated in figure 3(f) and around this region the device is evidently not in a favorable regime. In the purple shaded region of figure 3(d) the illuminated source-drain current is always less than the dark current giving a negative photocurrent. Indeed, graphene is hole doped in the dark and becomes less hole doped when illuminated with the inflow of photoelectrons from InSe (figure 3(e)). In the pink shaded region of figure 3(d) on the contrary, the illuminated source-drain current is always more than the dark current giving a positive photocurrent because graphene is electron doped in the dark and becomes more electron doped when illuminated again due to an inflow of photoelectrons from InSe (figure 3(g)).

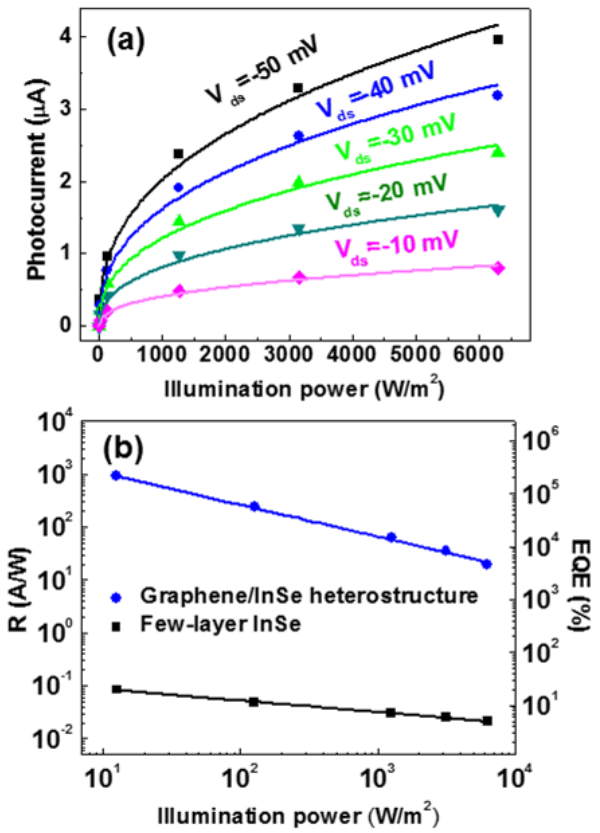

Figure 4. (a) Photocurrent as a function of illumination power for different source-drain voltages in the graphene/20-layer InSe heterostructure. Symbols: experimental data, continuous lines: parameterized fit of relation (3). (b) R and EQE as a function of illuminated power for a graphene/20-layer InSe heterostructure and a 20-layer InSe homostructure. Symbols: experimental data, continuous lines: parameterized fit of relation (4).

The variation of the photocurrent with illumination power is extracted from the data of figure 3(c) and shown in figure 4(a). This variation can be used to parameterize our device. The photocurrent can generally be expressed as:[33,34]

$$I_{ph} = WC_i \mu \Delta V_G V_{ds} / L \quad (1)$$

where C_i is the total capacitance of the gate dielectric and few-layer InSe per unit area, μ is the carrier mobility of graphene, ΔV_G is shift of the voltage at the Dirac point of graphene, W and L are the width and the length of the channel, respectively. In addition, ΔV_G has a non-linear power law dependence on the illumination power which can be fitted phenomenologically[33,34]:

$$\Delta V_G = \alpha P^{\beta} \quad (2)$$

where P is the illumination power density per unit surface, and α and β are parameters. Using relations (1) and (2) we can extract the dependence of the photocurrent on two critical parameters: the source-drain voltage and the illumination power density:

$$I_{ph} = \alpha WC_i \mu V_{ds} P^{\beta} / L = \gamma V_{ds} P^{\beta} \quad (3)$$

where γ is a dimensional parameter characterizing the device. Relation (3) shows the dependence of I_{ph} on both V_{ds} and P and is used to parameterize the dataset of figure 4(a) giving $\beta \approx 0.39$.

What is the gain in quantum efficiency in going from few-layer InSe to the graphene/InSe heterostructure? In figure 4(b) we compare the two structures (the same thickness of few-layer InSe device was also fabricated, see ESI, Fig. S4†) by computing the photoresponsivity (R) and external quantum efficiency (EQE) as a function of illuminated power ranging between 12.6 W/m^2 to 6.3×10^3 W/m^2 (for reference, polychromatic solar radiation at the earth's surface is roughly 10^3 W/m^2). $R = I_{ph} / (P \times S)$ is defined as the photocurrent (I_{ph}) generated per unit power (P) of incident light on the effective area of the photo-detector (S). $EQE = hcR / (e\lambda)$ is

the number of photoexcited electron-hole pairs per absorbed photon and is directly proportional to R. Under the same illumination condition (532 nm wavelength unfocussed laser light at a power density of 12.6 W/m^2) we obtain for the graphene/InSe heterostructure $R = 0.94 \times 10^3$ A/W and $EQE = 2.18 \times 10^5$ % with $V_{ds} = $ -50 mV and $V_g = 0$ V. This is four orders of magnitude higher than the values of $R = 0.101$ A/W and $EQE = 23.5$ % in the few-layer InSe device with $V_{ds} = 5$ V and $V_g = 0$ V. In the case of the heterostructure, the enhanced EQE represents the gain in efficiency but not the number of photoexcited pairs per absorbed photon anymore since the photocurrent is generated by a different mechanism. As expected, the efficiency decreases as the incident power increases. This variation follows a power law by taking eqn (3) into account:

$$R = I_{ph} / (P \times S) = \gamma V_{ds} P^{\beta} / (P \times S) = \gamma V_{ds} P^{\beta - 1} / S \quad (4)$$

and we find the exponents $\beta \approx 0.39$ and $\beta \approx 0.78$ for the graphene/InSe heterostructure and few-layer InSe respectively. It is worthwhile to note that the values of R and EQE depend critically on the conditions of measurement as seen in eqn (4). R increases linearly with V_{ds} but in particular can be increased greatly at very low power as seen by the inverse dependence in relation (4). For example, if we refer to figure 4(a), dI_{ph} / dP is nearly 50 times higher at an illumination of 12.6 W/m^2 compared to an illumination of 6.3 $\times$ 10^3 W/m^2. Clearly the heterostructure is a spectacular improvement with respect to the homostructural few-layer InSe device which has similar absorption and photoelectron generation but with R and EQE four orders of magnitude lower.

Adding a graphene monolayer provides very efficient transport of the photoelectrons as compared to InSe where recombination is high except in areas within nanometric distances from the source and drain contacts. Since the InSe layer is only a few nanometers thick, photoelectrons from the whole volume can be potentially extracted vertically into the graphene layer. Graphene is not an efficient photo-detector, with high dark current and low absorption and photoresponsivity. However when InSe is used for generating photoelectrons we have seen that the generated charge is enough to produce significant changes in the Fermi level of the adjacent graphene monolayer. Finally we have also shown that the graphene layer spectacularly enhances the performance not only through its electronic properties but also as a protective packaging for the InSe layers conferring ambient condition compatibility to the device. A possible improvement to this device is to use a dry transfer process to achieve better interface conditions between graphene and the semiconductor layer.

In summary, we fabricate a monolayer graphene/few-layer InSe heterostructure photo-detector by transferring anodic bonded graphene on top of mechanically exfoliated few-layer InSe. This hybrid device shows a four orders of magnitude enhancement in photoresponsivity and external quantum efficiency with respect to a simple few-layer InSe device in working conditions of low source-drain voltage and high incident power. By adjusting the gate voltage the device can perform either with holes or with electrons with a photocurrent of the order of a microampere. This kind of performance, earlier seen in TMDC based heterostructures is possible thanks to the combination of absorption and photoelectron generation characteristics of InSe and efficient

charge transport in graphene. Importantly we also show that the covering graphene layer acts as a protection for ultra-thin InSe and can therefore be used for other materials which are chemically unstable in ambient conditions.

ACKNOWLEDGMENT

This work was partly supported by French ANR project (Grant No. ANR-11-BS04-0019), by LABEX MATISSE through a post-doctoral grant and a scholarship from China Scholarship Council (CSC, Grant No. 2011618135). We acknowledge the "Consortium des salles blanches d'Ile de France" for access to clean room facilities. We acknowledge M. Rosticher, J. Palomo and A. Paradisi for help with clean room work, J. Li for TEM experiment, D. Taverna for TEM data interpretation and A. Chevy for the precursor materials used in this work.

ASSOCIATED CONTENT

†Electronic supplementary information (ESI) available: Fabrication process of a graphene/few-layered InSe heterostructure; characterization and measurement of a graphene/few-layer InSe photo-detector; degradation of 20-layer InSe under ambient conditions; Raman characterization of doping in graphene; the performance of a few-layer InSe photo-detector; and the schematic comparison of two devices. See DOI: 10.1039/c5nr00400d

AUTHOR INFORMATION

Corresponding Author

*Email: abhay.shukla@impmc.upmc.fr.

Notes

The authors declare no competing financial interest.

REFERENCES

1 K. S. Novoselov, A. K. Geim, S. V. Morozov, D. Jiang, Y. Zhang, S. V. Dubonos, I. V. Grigorieva and A. A. Firsov, *Science*, 2004, **306**, 666-669.

2 F. Schwierz, *Nat. Nanotechnol.*, 2010, **5**, 487-496.

3 B. Radisavljevic, A. Radenovic, J. Brivio, V. Giacometti and A. Kis, *Nat. Nanotechnol.*, 2011, **6**, 147–150.

4 M. Chhowalla, H. S. Shin, G. Eda, L. Li, K. P. Loh and H. Zhang, *Nat. Chem.*, 2013, **5**, 263–275.

5 F. Xia, T. Mueller, Y. Lin, A. Valdes-Garcia and P. Avouris, *Nat. Nanotechnol.*, 2009, **4**, 839–843.

6 T. Mueller, F. Xia and P. Avouris, *Nat. Photonics*, 2010, **4**, 297–301.

7 W. Zhang, J. K. Huang, C. H. Chen, Y. H. Chang, Y. J. Cheng and L. J. Li, *Adv. Mater.*, 2013, **25**, 3456–3461.

8 N. Perea-López, A. L. Elías, A. Berkdemir, A. Castro-Beltran, H. R. Gutiérrez, S. Feng, R. Lv, T. Hayashi, F. López-Urías, S. Ghosh, B. Muchharla, S. Talapatra, H. Tereones and M. Terrones *Adv. Funct. Mater.*, 2013, **23**, 5511–5517.

9 O. Lopez-Sanchez, D. Lembke, M. Kayci, A. Radenovic and A. Kis, *Nat. Nanotechnol.*, 2013, **8**, 497–501.

10 K. F. Mak, C. Lee, J. Hone, J. Shan and T. F. Heinz, Phys. *Rev. Lett.*, 2010, **105**, 136805.

11 G. Konstantatos, M. Badioli, L. Gaudreau, J. Osmond, M. Bernechea, F. P. Garcia de Arquer, F. Gatti and F. H. L. Koppens, *Nat. Nanotechnol.*, 2012, **7**, 363–368.

12 W. Zhang, C. P. Chuu, J. K. Huang, C. H. Chen, M. L. Tsai, Y. H. Chang, C. T. Liang, Y. Z. Chen, Y. L. Chueh, J. H. He, M. Y. Chou and L. J. Li, *Sci. Rep.*, 2014, **4**, 3826.

13 K. Roy, M. Padmanabhan, S. Goswami, T. P. Sai, G. Ramalingam, S. Raghavan and A. Ghosh, *Nat. Nanotechnol.*, 2013, **8**, 826–830.

14 S. R. Tamalampudi, Y. Y. Lu, R. Kumar U., R. Sankar, C. D. Liao, K. Moorthy B., C. H. Cheng, F. C. Chou and Y. T. Chen, *Nano Lett.*, 2014, **14**, 2800–2806.

15 S. Lei, L. Ge, S. Najmaei, A. George, R. Kappera, J. Lou, M. Chhowalla, H. Yamaguchi, G. Gupta, R. Vajtai, A. D. Mohite and P. M. Ajayan, *ACS Nano*, 2014, **8**, 1263–1272.

16 G. W. Mudd, S. A. Svatek, T. Ren, A. Patanè, O. Makarovsky, L. Eaves, P. H. Beton, Z. D. Kovalyuk, G. V. Lashkarev, Z. R. Kudrynskyi and A. I. Dmitriev, *Adv. Mater.*, 2013, **25**, 5714–5718.

17 K. Geim and I. V. Grigorieva, *Nature*, 2013, **499**, 419–425.

18 S. Böhm, *Nat. Nanotechnol.*, 2014, **9**, 741–742.

19 J. Huh, S. H. Kim, J. H. Chu, S.Y. Kim, J. H. Kim and S. Kwon, *Nanoscale*, 2014, **6**, 4379–4386.

20 A. Shukla, R. Kumar, J. Mazher and A. Balan, *Solid State Commun.*, 2009, **149**, 718–721.

21 K. Gacem, M. Boukhicha, Z. Chen and A. Shukla, *Nanotechnol.*, 2012, **23**, 505709.

22 Z. Chen, K. Gacem, M. Boukhicha, J. Biscaras and A. Shukla, *Nanotechnol.*, 2013, **24**, 415708.

23 G. F. Schneider, V. E. Calado, H. Zandbergen, L. M. K. Vandersypen and C. Dekker, *Nano Lett.*, 2010, **10**, 1912–1916.

24 T. Ikari, S. Shigetomi and K. Hashimoto, *Phys. stat. sol. (b)*, 1982, **111**, 477–481.

25 A. M. Mancini, G. Micocci and A. Rizzo, *Mater. Chem. Phys.*, 1983, **9**, 29-54.

26 C. Carlone, S. Jandl and H. R. Shanks, *Phys. stat. sol. (b)*, 1981, **103**, 123–130.

27 S. Ashokan, K. P. Jain, M. Balkanski and C. Julien, *Phys. Rev. B*, 1991, **44**, 11133.

28 J. Y. Tan, A. Avsar, J. Balakrishnan, G. K. W. Koon, T. Taychatanapat, E. C. T. O'Farrell, K. Watanabe, T. Taniguchi, G. Eda, A. H. Castro Neto and B. Özyilmaz, *Appl. Phys. Lett.*, 2014, **104**, 183504.

29 S. M. Atakishiev, D. Sh. Abdinov and G. A. Akhundov, *Phys. stat. sol. (b)*, 1968, **28**, K47–K50.

30 R. Mamy, X. Zaoui, J. Barrau and A. Chevy, *Revue Phys. Appl.*, 1990, **25**, 947–950.

31 R. Yan, Q. Zhang, W. Li, I. Calizo, T. Shen, C. A. Richter, R. Angela, A. R. Hight-Walker, X. Liang, A. Seabaugh, D. Jena, H.G. Xing, D. J. Gundlach and N. V. Nguyen, *Appl. Phys. Lett.*, 2012, **101**, 022105.

32 T. S. Lin and C. T. Lee, *Appl. Phys. Lett.*, 2012, **101**, 221118.

33 Z. Sun, Z. Liu, J. Li, G. A. Tai, S. P. Lau and F. Yan, *Adv. Mater.*, 2012, **24**, 5878–5883.

34 H. Xu, J. Wu, Q. Feng, N. Mao, C. Wang and J. Zhang, *Small*, 2014, **10**, 2300–2306. (3) Radisavljevic, B.; Radenovic, A.; Brivio, J.; Giacometti, V.; Kis, A. *Nat. Nanotechnol.* **2011**, *6*, 147–150.